

Fall October 28, 2016

Femtosecond pulse trains of polychromatic inverse Compton γ -rays from designer electron beams produced by laser-plasma acceleration in plasma channels

Serge Y Kalmykov

Isaac Ghebregziabher

X. Davoine, *CEA, DAM DIF*

Remi Lehe, *Lawrence Berkeley National Laboratory*

Agustin F. Lifschitz, et al.



This work is licensed under a [Creative Commons CC BY](https://creativecommons.org/licenses/by/4.0/) International License.



Femtosecond pulse trains of polychromatic inverse Compton γ -rays from designer electron beams produced by laser-plasma acceleration in plasma channels

S. Y. Kalmykov, I. A. Ghebregziabher, X. Davoine, R. Lehe, A. F. Lifschitz, V. Malka, and B. A. Shadwick

Citation: [AIP Conference Proceedings](#) **1777**, 080007 (2016); doi: 10.1063/1.4965664

View online: <http://dx.doi.org/10.1063/1.4965664>

View Table of Contents: <http://scitation.aip.org/content/aip/proceeding/aipcp/1777?ver=pdfcov>

Published by the [AIP Publishing](#)

Articles you may be interested in

[Compact tunable Compton x-ray source from laser-plasma accelerator and plasma mirror](#)

Phys. Plasmas **22**, 023106 (2015); 10.1063/1.4907655

[X-ray generation via laser Compton scattering using quasi-monoenergetic electron beam driven by laser-plasma acceleration](#)

AIP Conf. Proc. **1507**, 304 (2012); 10.1063/1.4773712

[Observation of pulsed x-ray trains produced by laser-electron Compton scatterings](#)

Rev. Sci. Instrum. **80**, 123304 (2009); 10.1063/1.3272789

[Design Considerations for Converting Laser-Accelerated Electron Beams into Brilliant X-Ray, \$\gamma\$ -Ray and Neutron-Beams](#)

AIP Conf. Proc. **802**, 6 (2005); 10.1063/1.2140617

[Observation of a highly directional \$\gamma\$ -ray beam from ultrashort, ultraintense laser pulse interactions with solids](#)

Phys. Plasmas **6**, 2150 (1999); 10.1063/1.873466

Femtosecond Pulse Trains of Polychromatic Inverse Compton γ -Rays from Designer Electron Beams Produced by Laser-Plasma Acceleration in Plasma Channels

S. Y. Kalmykov*, I. A. Ghebregziabher[†], X. Davoine**, R. Lehe[‡],
A. F. Lifschitz[‡], V. Malka[‡] and B. A. Shadwick*

*Department of Physics and Astronomy, University of Nebraska - Lincoln, Lincoln, NE 68588-0299, USA

[†]1845 F Street, Lincoln, NE 68508, USA

**CEA, DAM, DIF, Arpajon F-91297, France

[‡]Laboratoire d'Optique Appliquée, ENSTA-CNRS-École Polytechnique UMR 7639, Palaiseau F-91761, France

Abstract. Propagating a short, relativistically intense laser pulse in a plasma channel makes it possible to generate clean comb-like electron beams – sequences of synchronized, low phase-space volume bunches with controllable energy spacing [S. Y. Kalmykov *et al.*, “Accordion Effect Revisited: Generation of Comb-Like Electron Beams in Plasma Channels,” in *Advanced Accelerator Concepts: 16th Workshop*, AIP Conference Proceedings; this volume]. All-optical control of the electron beam phase space structure via manipulation of the drive pulse phase (negative chirp) and parameters of the channel enables the design of a tunable, all-optical source of polychromatic pulsed γ -rays using the mechanism of inverse Compton scattering.

Keywords: Laser wakefield acceleration, blowout, plasma channel, electron beam shaping, inverse Compton scattering, PIC simulations

PACS: 41.75.Jv, 41.85.Ct, 52.35.Mw, 52.38.Hb, 52.38.Kd, 52.38.Ph, 52.65.Rr, 52.65.Ww

INTRODUCTION

Relativistic optical phenomena [1] are essential for production and shaping of electron beams in laser-plasma accelerators (LPAs). In particular, it is possible to generate trains of fs-length bunches with a low phase space volume and controlled separation in energy [2–5]. These comb-like beams may find a unique application as drivers of all-optical γ -ray sources [6–11] based on the inverse Compton scattering (ICS) mechanism [12–14]. The production of bright, ps-duration ICS γ -rays has been earlier demonstrated with head-on collisions of intense laser pulses and electron beams from conventional accelerators [15–22]. These γ -rays, which are well collimated, quasi-monochromatic (QM), and have a high degree of polarization, are attractive as electron beam diagnostics [15]. ICS γ -rays are also employed in the generation of polarized positrons from dense targets [17] and to demonstrate nuclear fluorescence [19–21]. Nuclear photonics applications benefit from the portability and unprecedented degree of control over the radiation spectrum afforded by an all-optical γ -ray source. In effect, the structure of the electron beam phase space imprints into the ICS γ -ray spectra. The electron beam, in turn, is the product of the nonlinear optical evolution of a relativistically intense laser pulse, which drives the wake in an underdense plasma, $\omega_p \ll \omega_0$ [where $\omega_p = (4\pi e^2 n_0 / m_e)^{1/2}$ is the Langmuir electron frequency, ω_0 is the pulse carrier frequency, n_0 is the background electron density, $-|e|$ and m_e are the electron charge and rest mass]. The radiation pressure of the pulse creates an electron density cavity (“bubble”) that evolves in lock-step with the optical driver, making it possible to trap ambient plasma electrons, eliminating the need for an external photocathode [23]. Propagating the pulse in an external plasma channel may, under the right circumstances, destabilize the bubble, bringing about oscillations of its size (*the accordion effect*) and periodic self-injection, shaping the electron beam into a synchronized sequence of QM bunches with a 100 pC-scale charge [2–5]. Unwanted continuous self-injection (a.k.a. dark current) and accumulation of a massive low-energy tail can be suppressed by using a *negatively chirped drive pulse* (NCP) with a bandwidth close to a one-half of the carrier wavelength [4, 5, 24]. Changing the NCP length (as permitted by the large bandwidth) and the channel radius enables control over the number of components in the energy comb and, hence, in the spectrum of polychromatic ICS γ -rays.

We show in this report that proposed all-optical manipulations enable controlled generation of GeV-scale, synchronized trains of high-quality electron bunches, enabling the design of a compact, tunable, all-optical source of polychromatic γ -rays, a unique scientific instrument with a broad range of applications.

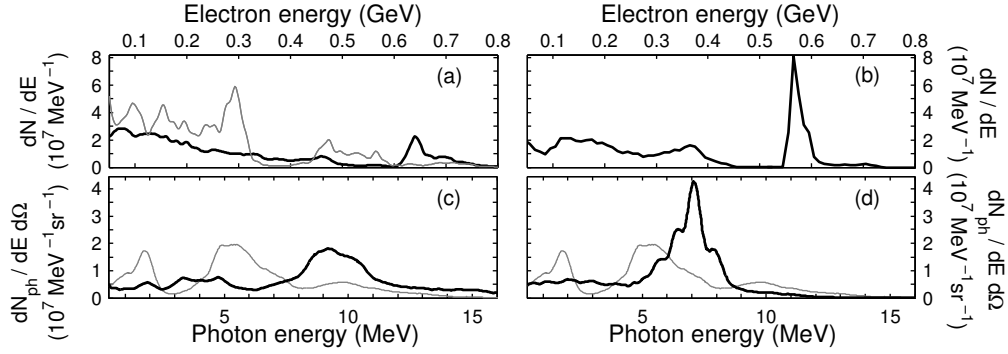


FIGURE 1. QM electron beams at dephasing and their ICS signals. (a), (b) Electron energy spectra [5]; (c), (d) γ -ray spectra (gray: the reference case). (a), (c) 30 fs NCP in a uniform plasma. (b), (d) 20 fs NCP in a channel matched to the spot size of the incident pulse. Electron beam statistics are shown in Table 1.

INTERACTION REGIMES AND SIMULATION METHODS

Accurate self-consistent simulations of electron phase space dynamics in the LPA are carried out with the fully explicit, quasi-cylindrical, three-dimensional (3D) particle-in-cell (PIC) code CALDER-Circ [25]. The code uses a numerical Cherenkov-free electromagnetic solver [26] and third-order splines for the macroparticles. These features, in combination with fine grid ($\Delta z = \Delta r / 16 = 0.125c / \omega_0 = 16$ nm, where $r^2 = x^2 + y^2$) and large number of particles per cell (20) maintain low sampling noise, negligible numerical dispersion, and also avoid numerical emittance dilution.

The plasma spans from $z=0$ to 3 mm, having 0.5 mm linear entrance and exit ramps, and a 2 mm flat section with the density 6.5×10^{18} cm $^{-3}$. A linearly polarized, 70 TW pulse with the carrier wavelength $\lambda_0 = 0.805$ μ m propagates in the positive z -direction. The normalized vector potential in the focal plane is Gaussian, $a(z=0) = a_0 \exp[-(r/r_0)^2 - 2 \ln 2 (t/\tau_L)^2 + i\varphi(t)]$, with $a_0 = 3.27$ and $r_0 = 13.6$ μ m. The phase variation defines the instantaneous frequency, $\omega(t) = -d\varphi/dt = \omega_0 - (4 \ln 2)(\kappa/\tau_L)^2 t$, where $\omega_0 = 2\pi c/\lambda_0$. The simulation with a 30 fs-length, transform-limited pulse ($\tau_L = 30$ fs, $\kappa = 0$), is referred to as *the reference case* [24]. To suppress diffraction of the pulse leading edge and to controllably obtain comb-like electron beams, we introduce a parabolic leaky channel [5]. To avoid pulse self-steepening in the course of propagation in a plasma, we introduce a frequency bandwidth equivalent to a 5 fs transform-limited duration, and temporally advance the higher frequencies. The results presented below correspond to a 30 fs NCP ($\kappa = 2.4323$) propagating in a uniform plasma and in a channel matched to the self-guided spot size and to a 20 fs NCP ($\kappa = 1.968$) propagating in a channel matched to the spot size of the incident pulse. Details of electron beam shaping process and statistics of the resulting “designer” beams are reported elsewhere [5].

The ICS simulations are performed using a single-particle-trajectory tracking, 3D relativistic code [27]. The ICS spectra are modeled directly by extracting N_b PIC macroparticles (electrons) from the first and second buckets of the wake and using their coordinates and momenta to sample the six-dimensional phase space of electrons. Electrons with thus specified initial conditions are then propagated in a free space by solving the relativistic equations of motion. In the absence of the laser field, their trajectories are ballistic. Since the electron beams considered here are relativistic and have low density ($n_e \langle \gamma_e \rangle^{-3} \ll 10^{16}$ cm $^{-3}$), space charge forces are neglected [12, 13]. Radiation damping is also

TABLE 1. Statistics of electron beams at dephasing (Fig. 1). z_d is the dephasing length; Q is the charge; $\langle E \rangle$ is the mean energy; σ_E is the dispersion of energy; σ_α is the RMS divergence [4]; ε_\perp^N is the RMS normalized transverse emittance [4]; $\langle F \rangle = Q/\sigma_E$ is the average flux; τ_b is an RMS bunch duration. Statistics of the tails are collected in the energy intervals 50 MeV $< E < E_{\text{cut}}$, where $E_{\text{cut}} = 600$ MeV for the 30 fs NCP; 500 MeV for the 20 fs NCP; and 385 MeV in the reference case.

	z_d [mm]	Q [pC]	$\langle E \rangle$ [MeV]	σ_E [MeV]	σ_α [mrad]	ε_\perp^N [mm mrad]	$\langle F \rangle$ [pC MeV $^{-1}$]	τ_b [fs]
NCP, 30 fs, QM	2.36	205	675	38.0	1.75	0.485	5.40	2.25
NCP, 20 fs, QM	2.16	375	575	15.5	2.43	0.760	24.25	4.35
Reference, QM	2.16	275	505	45.0	1.95	0.500	6.10	3.40
NCP, 30 fs, tail	2.36	1025	225	133	6.66	—	7.75	—
NCP, 20 fs, tail	2.16	733	225	104	7.95	—	7.08	—
Reference, tail	2.16	1520	200	81.5	10.45	—	18.75	—

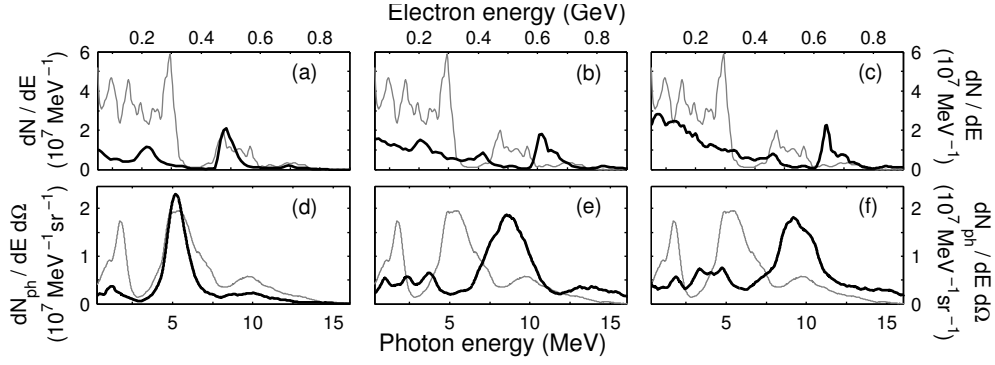


FIGURE 2. A 30 fs NCP propagating in a uniform plasma: evolution of electron and ICS γ -ray spectra through dephasing. (a)–(c) Electron energy spectra; (d)–(f) γ -ray spectra (gray: the reference case at dephasing). (a), (d) $z = 1.72$ mm; (b), (e) 2.16 mm (point of dephasing in the reference case); (c), (f) $z_d = 2.36$ mm. The negative chirp of the driver doubles the photon energy, while preserving the flux in signal and avoiding accumulation of the background.

neglected, as the energy emitted by an electron passing through the interaction laser pulse (ILP) is small compared to the energy of the electron. The electron beam collides head-on with the linearly polarized ILP, which has a carrier wavelength $0.8 \mu\text{m}$ (hence the interaction photon energy $E_{\text{int}} = 1.5 \text{ eV}$), 250 fs duration, and $20 \mu\text{m}$ focal spot size. The ILP is treated in the paraxial approximation. Timing between the electron beam and the ILP is chosen so that the beam and the peak of the ILP intensity arrive at the ILP focal plane simultaneously. As the ILP is shorter than 5% of its Rayleigh length, and the electron beam spot size is in the sub-micron range, the interaction occurs in an almost planar-wave geometry. To avoid broadening the ICS spectra [28, 29], a linear interaction regime is chosen, with the ILP normalized vector potential $a_{\text{int}} = 0.1$. Once the orbits of individual electrons are obtained, the energy density radiated per unit frequency ω and solid angle Ω per electron by the ensemble is obtained by

$$\frac{d^2 I_e}{d\omega d\Omega} = \frac{1}{N_b} \left(\frac{e^2 \omega^2}{4\pi^2 c} \right) \sum_{i=1}^{N_b} \left| \int_{-\infty}^{\infty} \mathbf{n} \times (\mathbf{n} \times \boldsymbol{\beta}_i) \exp \left\{ i\omega \left(t - \frac{\mathbf{n} \cdot \mathbf{r}_i(t)}{c} \right) \right\} dt \right|^2,$$

where \mathbf{n} is the unit observation vector (pointing in the direction of electron beam propagation), and \mathbf{r}_i and $\boldsymbol{\beta}_i = \mathbf{v}_i/c$ are the radius vector and normalized velocity of the test electron, respectively. The net energy radiated by the beam is then given by $d^2 I_{\text{tot}}/d\omega d\Omega = (Q/e)d^2 I_e/d\omega d\Omega$, where Q is the beam charge.

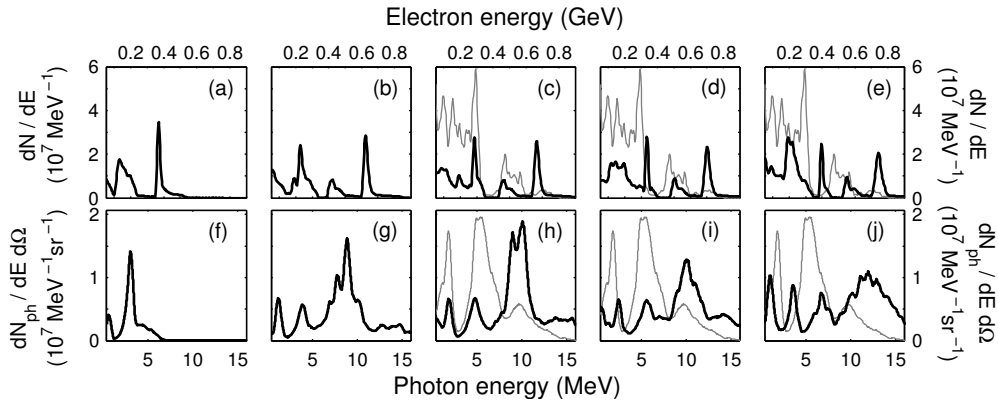


FIGURE 3. A 30 fs NCP propagating in a channel matched to the self-guided spot size: evolution of the energy comb ICS γ -ray spectra through dephasing. (a)–(e) Electron energy spectra [5]; (f)–(j) γ -ray spectra (gray: the reference case at dephasing). (a), (f) $z = 1.48$ mm; (b), (g) 2.08 mm; (c), (h) 2.16 mm (the point of dephasing in the reference case); (d), (i) 2.32 mm; and (e), (j) $z_d = 2.48$ mm.

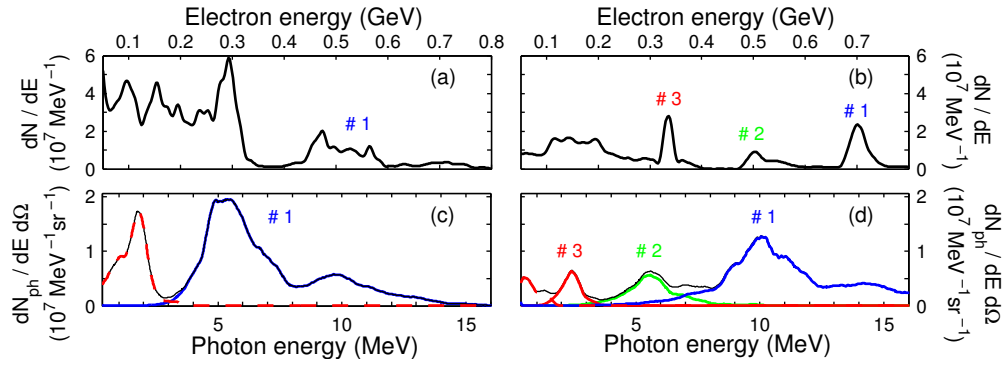


FIGURE 4. (Color online) Partial contributions of electron beam components to the ICS spectrum. (a), (b) Electron spectra. (c), (d) γ -ray spectra (thin black line shows the sum of partial signals). (a), (c) Reference case. (b), (d) a 30 fs NCP propagating in a channel matched to the self-guided spot size, $z = 2.32$ mm (statistics of individual electron bunches are shown in Table 2). Dashed lines in panel (c), (d) depict the signal from the electron energy tail, (c) $50 \text{ MeV} < E < 385 \text{ MeV}$, (d) $50 \text{ MeV} < E < 300 \text{ MeV}$.

RESULTS AND DISCUSSION

The negative chirp of the drive pulse reduces the level of dark current and delays electron dephasing in the LPA [24]. Figures 1(a) and (b) and statistics collected in Table 1 demonstrate these effects in a uniform plasma and in a plasma channel [5]. An energy tail, containing 85% of charge accelerated beyond 50 MeV, dominates the spectrum in the reference case. The chirp and the channel bring the tail down, reducing its average flux by a factor 2.5. As a result, the peaks centered around $E_{\text{ph}} \approx 4\langle\gamma_e\rangle^2 E_{\text{int}}$ become dominant in the ICS spectra [cf. Figs. 1(c) and (d)]. Yet a mrad-scale electron beam divergence keeps them rather broad ($\sim 30\%$ energy spread). Interestingly, compressing the NCP to 20 fs and propagating it in a channel increases the electron beam brightness so significantly as to double the γ -ray signal, while keeping the noise level almost unaltered. Figures 2(a)–(c) show that an electron beam, accelerated with a 30 fs NCP through dephasing in a uniform plasma, accumulates only a minimal amount of noise, while receiving $\sim 30\%$ energy boost compared to the reference case. As seen in Fig. 2(a), the maximum energy gain achievable with the transform-limited pulse can be reached with the NCP in a 20% shorter plasma, with the low-energy background reduced by 80% [5]. The corresponding ICS spectrum in Fig. 2(d) lacks the tail almost entirely (in striking contrast to the reference case), and has its bandwidth reduced by nearly half. Figures 2(d)–(f) demonstrate γ -ray energy doubling, with the flux and energy spread of the signal preserved, and the background remaining at a fairly low 25% level.

In contrast to the uniform plasma, acceleration through dephasing in a channel (with the 30 fs NCP) yields a triplet of synchronized, low phase-space volume bunches with controllable energy spacing [cf. Figs. 3(a)–(e)]. The tricolor beam evolves through dephasing accumulating noise very slowly, without deteriorating the polychromatic ICS signal [cf. Figs. 3(f)–(j)]. The energy of individual bunches can be thus safely varied within a broad interval. However, as soon as the electron energy exceeds 700 MeV, the mrad-scale electron beam divergence starts degrading the ICS signal, as is clearly seen in examination of the highest energy spectral component in Fig. 3(j). In this situation, extending the photon energy beyond 10 MeV without compromising the beam quality may need substantial increase of ILP frequency (e.g., frequency-doubling [11]). ICS spectra in Figs. 3(f)–(j) reveal distinct QM features corresponding to the peaks in electron energy spectra. In effect, Figs. 4(b) and (d) indicate that individual electron bunches making up the comb (with the statistics collected in Table 2) do produce background-free QM γ -ray signals centered at theoretically predicted energies, with a $\sim 30\%$ relative energy spread. These fs-length flashes of different colors ($E_{\text{ph}} = 2.6, 5.5,$ and 10 MeV) have respective time delays of the order a few fs. The electron energy tail [extending below 300 MeV in Fig. 4(b)] contributes to the photon energies below 1.5 MeV, which is outside the range of the γ -ray energy comb.

TABLE 2. Statistics of partial electron beams from Fig. 4(b).

	Q [pC]	$\langle E \rangle$ [MeV]	σ_E [MeV]	σ_α [mrad]	ε_\perp^N [mm mrad]	$\langle F \rangle$ [pC MeV $^{-1}$]	τ_b [fs]
Beam 1	157.5	710	21.5	2.60	1.22	7.33	1.45
Beam 2	82.5	524	28.5	3.45	1.23	2.90	1.14
Beam 3	105	345	16.0	4.05	0.72	6.55	1.50

SUMMARY AND OUTLOOK

Inverse Compton scattering of an optical beam by GeV-scale electrons accelerated in laser wakefield underlies the design of an all-optical γ -ray source. Such a source can be controlled by manipulation of the electron beam phase space via relativistic optical effects. Looking forward to the arrival of PW-class laser systems delivering sub-2-cycle pulses [30], we use their ultrahigh bandwidth to modify the electron beam phase space structure. First, manipulations of the drive pulse phase (negative chirp) improve the monochromaticity and boost the energy of 10 MeV-scale γ -rays. Secondly, propagating the pulse in a plasma channel may destabilize the accelerating bucket (laser-driven electron bubble), causing oscillations in its size. This *accordion effect* [5] causes periodic self-injection of ambient electrons and their subsequent acceleration without quality degradation, while the negative chirp of the driver reduces the pollution of electron spectra by a low-energy background. The first-principles numerical simulations show that, due to the low phase space volume, clear separation of spectral components in energy, and a minimal amount of noise, the comb-like electron beams can drive compact, tunable, multi-color ICS γ -ray sources that can find applications in nuclear photonics and radiography [19–21]. Natural mutual synchronization of fs-length electron bunches and γ -ray flashes may be an asset to pump-probe experiments and laboratory modeling of single-event effects.

ACKNOWLEDGMENTS

Work of SYK and BAS was supported by the US Department of Energy Grant DE-SC0008382 and the National Science Foundation Grant PHY-1104683. Inverse Compton scattering simulations were completed utilizing the Holland Computing Center of the University of Nebraska. The CALDER-Circ simulations of this work were performed using HPC resources of GENCI-CCRT and GENCI-CINES (grant 2013-057027).

REFERENCES

1. G. A. Mourou, T. Tajima, and S. V. Bulanov, *Rev. Mod. Phys.* **78**, 309–371 (2006).
2. A. Oguchi *et al.*, *Phys. Plasmas* **15**, 043102 (2008).
3. A. Zhidkov *et al.*, *Phys. Plasmas* **17**, 083101 (2010).
4. S. Y. Kalmykov, B. A. Shadwick, and X. Davoine, “All-optical control of electron trapping in plasma channels,” in *2013 19th IEEE Pulsed Power Conference (PPC)*, pp. 1–6; DOI: 10.1109/PPC.2013.6627518.
5. S. Y. Kalmykov *et al.*, “Accordion Effect Revisited: Generation of Comb-Like Electron Beams in Plasma Channels,” in *Advanced Accelerator Concepts: 16th Workshop*, edited by M. Hogan, AIP Conference Proceedings; this volume.
6. H. Schwoerer *et al.*, *Phys. Rev. Lett.* **96**, 014802 (2006).
7. K. Ta Phuok *et al.*, *Nat. Photon.* **6**, 308–311 (2012).
8. S. Chen *et al.*, *Phys. Rev. Lett.* **110**, 155003 (2013).
9. E. Miura *et al.*, *Appl. Phys. Express* **7**, 046701 (2014).
10. N. D. Powers *et al.*, *Nat. Photon.* **8**, 28–31 (2014).
11. C. Liu *et al.*, *Opt. Lett.* **39**, 4132–4135 (2014).
12. E. Esarey, S. K. Ride, and P. Sprangle, *Phys. Rev. E* **48**, 3003–3021 (1993).
13. S. K. Ride, E. Esarey, and M. Baine, *Phys. Rev. E* **52**, 5425–5442 (1995).
14. F. Albert *et al.*, *Phys. Rev. ST Accel. Beams* **14**, 050703 (2011).
15. M. Baylac *et al.*, *Phys. Lett. B* **539**, 8–12 (2002).
16. I. Sakai *et al.*, *Phys. Rev. ST Accel. Beams* **6**, 091001 (2003).
17. T. Omori *et al.*, *Phys. Rev. Lett.* **96**, 114801 (2006).
18. K. Kawase *et al.*, *Nucl. Instrum. Methods in Phys. Res. A* **592**, 154–161 (2008).
19. N. Kikuzawa *et al.*, *Appl. Phys. Express* **2**, 036502 (2009).
20. T. Hayakawa *et al.*, *Rev. Sci. Instr.* **80**, 045110 (2009).
21. F. Albert *et al.*, *Phys. Rev. ST Accel. Beams* **13**, 070704 (2010).
22. A. Jochmann *et al.*, *Phys. Rev. Lett.* **111**, 114803 (2013).
23. S. Y. Kalmykov *et al.*, *Phys. Plasmas* **18**, 056704 (2011).
24. S. Y. Kalmykov *et al.*, *New J. Phys.* **14**, 033025 (2012).
25. A. F. Lifschitz *et al.*, *J. Comput. Phys.* **228**, 1803–1814 (2009).
26. R. Lehe *et al.*, *Phys. Rev. ST Accel. Beams* **16**, 021301 (2013).
27. I. Ghebregziabher, B. A. Shadwick, and D. P. Umstadter, *Phys. Rev. ST Accel. Beams* **16**, 030705 (2013).
28. Y. Y. Lau *et al.*, *Phys. Plasmas* **10**, 2155–2162 (2003).
29. C. Maroli *et al.*, *Phys. Rev. ST Accel. Beams* **16**, 030706 (2013).
30. Zs. Major *et al.*, *Rev. Laser Eng.* **37**, 431–436 (2009).